Dual effect of ZrO2 on phase separation and crystallization in Li2O-Al2O3-SiO2-P2O5 glasses

Lifan Zhu, Mingzhong Wang, Yinsheng Xu, Xianghua Zhang, Ping Lu

Dual effect of ZrO_2 on phase separation and crystallization in Li_2O-Al_2O_3-SiO_2-P_2O_5 glasses

Lifan Zhu,[1] Mingzhong Wang,[2] Yinsheng Xu[3], Xianghua Zhang[3,4], Ping Lu,[1, 3, *]

[1] School of Materials Science and Engineering, Wuhan University of Technology, Wuhan 430070, China

[2] Xianning CSG Photovoltaic Glass Co., Ltd., Xianning 437100, China

[3] State Key Laboratory of Silicate Materials for Architectures, Wuhan University of Technology, Wuhan 430070, China

[4] ISCR (Institut Des Sciences Chimiques de Rennes) - UMR 6226, CNRS, Univ Rennes, 35000 Rennes, France

*Corresponding author

Email: Lupingwh@whut.edu.cn; Phone: +86 13476073984

This article has been accepted for publication and undergone full peer review but has not been through the copyediting, typesetting, pagination and proofreading process, which may lead to differences between this version and the Version of Record. Please cite this article as doi: 10.1111/jace.18540.

Abstract

ZrO_2 is an effective nucleation agent for low-expansion lithium aluminum silicate (LAS) glass-ceramic (GC) with high Al_2O_3 content. However, the effect of ZrO_2 is still not fully understand in LAS glasses with low contents of Al_2O_3 and P_2O_5. In this work, the effect of ZrO_2 on the phase separation and crystallization of Li_2O-Al_2O_3-SiO_2-P_2O_5 glasses were investigated. The results revealed that ZrO_2 significantly increased T_g and the crystallization temperature of Li_2SiO_3 and $Li_2Si_2O_5$ crystals. Li_3PO_4 crystals precipitated preferentially in the glass containing 3.6 mol% ZrO_2 wherein Zr was stable in the network and no precipitation of ZrO_2 nanocrystals was observed. Moreover, the separation of phosphate-rich phases in the as-quenched glasses increased with the addition of ZrO_2. The findings of the study revealed a dual role of ZrO_2. First, ZrO_2 acted as a glass network former rather than a nucleation agent, increasing glass viscosity and the nucleation barrier of Li_2SiO_3 through its strong network connectivity. Secondly, as Zr preferentially combined with NBO to form Si-O-Zr linkages, a sufficient amount of charge-balancing Li^+ ions existed in the network, which promoted the separation of phosphate-rich phases. It indicated that the incorporation of ZrO_2 contributes to the activation of the nucleation role of P_2O_5, thus contribute to the formation of nanocrystals and fine microstructure of GCs.

Keywords: ZrO_2, glass ceramic, nucleation, phase separation, crystallization

.

1. Introduction

Since the pioneering work of Stookey in the 1950s,[1] much attention has been directed toward the development of glass ceramics (GCs). These materials exhibit highly desirable properties[2] which result from the combination of the advantages of their amorphous matrix and those of the microcrystalline phase dispersed throughout. The properties of GCs strongly depend on the nature and composition of their crystalline phases. Lithium aluminum silicate (LAS) GCs have been extensively studied owing to their low thermal expansion coefficients, high mechanical strength, and transparency characteristics. LAS glasses are widely used in fireplaces, telescope mirrors, and dental restorative materials.[3-5] Based on the phase diagram of LAS glass, crystals with different characteristics can be formed in situ by adjusting the glass composition.[6] In particular, the addition of nucleation agents such as ZrO_2 or P_2O_5,[7, 8] which form abundant uniform nucleation sites, allow for controlled crystallization to be achieved.

The effects of nucleation agents on crystallization are significantly influenced by the composition of the original glass; e.g., P_2O_5 promotes crystallization in LAS glasses with low Al_2O_3 contents, however crystallization is inhibited for high Al_2O_3 content.[9-11] ^{31}P solid-state nuclear magnetic resonance (NMR) analyses have indicated that this behavior is related to changes in the structural environment of phosphorus.[12, 13] In LAS glasses with low Al_2O_3 content, phosphorus is mainly present as orthophosphate segregated in the glass network

.

and promotes phase separation and crystallization. With increasing Al_2O_3 content, phosphorus combines with aluminum to form a POAl complex, and according to the aluminum avoidance principle (i.e., Loewenstein's Rule), phosphorus is evenly dispersed in the glass network, which inhibits crystallization.[14, 15] A similar dependence was observed for ZrO_2, which acts as an effective nucleation agent for low-expansion LAS GCs with high Al_2O_3 content,[16] thereby decreasing the crystallization temperature and promoting the precipitation of the β-quartz solid solution (ss). It was reported that Zr-rich liquid-liquid phase-separation droplets are transformed into ZrO_2 nanocrystals, serving as nucleation sites for the β-quartz ss.[17, 18] However, ZrO_2 inhibits crystallization in LAS glasses with low Al_2O_3 content. Khalkhali *et al.*[19] reported that ZrO_2 significantly increases the crystallization temperature of the LAS glasses, the final GCs are coarse. Additionally, ZrO_2 was found to completely inhibit crystallization in stoichiometric Li_2O-$2SiO_2$ glass and induce significant surface crystallization.[20]

For LAS glasses co-doped with ZrO_2 and P_2O_5, the effects of ZrO_2 are even more complex. Apel *et al.*[21] reported that for a multi-component $Li_2Si_2O_5$ glass (containing minor amounts of Al_2O_3, K_2O, and P_2O_5), ZrO_2 did not precipitate as nanocrystal nuclei or form crystalline phases, but increased the glass viscosity and hindered the growth of $Li_2Si_2O_5$ crystals. Krüger *et al.*[22] studied the nucleation kinetics of a similar $Li_2Si_2O_5$ glass where it was assumed that ZrO_2 accelerates the precipitation of amorphous orthophosphate phases which provides .

numerous heterogeneous nucleation sites. The effects of ZrO_2 in multi-component $Li_2Si_2O_5$-based glasses is not completely understood, particularly for glasses co-doped with ZrO_2 and P_2O_5.

Elucidating the intrinsic role of the nucleation agent will enable improved control of the crystallization of GCs and further enhancement of their properties. Herein, we examined the effects of ZrO_2 on crystallization in multi-component Li_2O-Al_2O_3-SiO_2-P_2O_5 glasses. Multi-stage thermal treatments were used to study the related phase-separation and crystallization behaviors. The crystalline phase and morphology of the heat-treated samples were analyzed by X-ray diffraction (XRD) and SEM, respectively. Because the effects of the nucleating agent strongly depend on the glass structure, Raman spectroscopy was used to investigate the origin of these effects from a structural perspective.

2. Experimental

2.1 Glass preparation

SiO_2 (99.98 %), Li_2CO_3 (99.90 %), Al_2O_3 (99.80 %), $NH_4H_2PO_4$ (≥99.0 %), and ZrO_2 (99.8 %) were used as starting materials. A standard melting-quenching technique was used to prepare glasses with nominal compositions (Table 1) of $x$$ZrO_2$-(100-$x$)(0.725$SiO_2-0.05Al_2O_3-0.215Li_2O-0.01P_2O_5$) ($x$ = 0, 1.8, 3.6 mol%), labeled as P1Z0, P1Z2, and P1Z4, respectively, and a P_2O_5-free glass with a composition of 73.5SiO_2-5Al_2O_3-21.5Li_2O (P0Z0; reference). For each composition, a 150 g batch was thoroughly mixed and melted at 1590 ° C for 3 h in a Pt-Rh .

(90/10 wt%) crucible. The melt was quenched by pouring onto a copper plate and then immediately pressed by a second plate to maximize the cooling rate.

Glass compositions (Table 1) were determined by X-ray fluorescence spectroscopy (XRF, PANalytical Axios, Netherlands), while Li_2O content was determined by atomic absorption spectrometry (AAS, CONTRAA-700, Analytik Jena, Germany). The relative errors of these two analytical methods were 0.05 and <0.01 mol%, respectively.

2.2 Heat treatment schedule

Differential scanning calorimetry (DSC) was used to determine the required heat treatment temperatures. As-quenched glasses were broken into small pieces prior to heat treatment and a heating rate of 10 ° C/min was applied. All samples were quenched to 25 ° C after heat treatment. The heat treatment conditions were listed in Table 2.

Schedule I. Nucleation. To investigate the effect of ZrO_2 on phase separation and nucleation, the samples were preheated within the typical range of nucleation temperatures, ~60 ° C above the glass transition temperature (T_g). P1Z0 was heated at 540 ° C for 2 and 4 h, P1Z2 was heated at 560 ° C for 2 and 4 h, and P1Z4 was heated at 580 ° C for 2 and 4 h.

Schedule II. Crystal growth. To study the effect of ZrO_2 on crystallization temperature, crystallization sequence, and crystallinity, P1Z0 was consecutively heated to 560, 620, 680, 700, 720, 750, 770, and 820 ° C, while .

P1Z4 was similarly heated to 630, 680, 720, 750, 790, 820, 870, and 900 ° C. Samples were held at each temperature for 10 min to monitor the crystalline phase evolution, prior to the subsequent temperature step.

Schedule Ⅲ. Primary phase evolution. To study the possible effect of ZrO_2 on the primary crystalline phase. P1Z0 was heated at 575 ° C for 10, 30, and 60 min, while P1Z4 was heated at 650 ° C for 10, 30, and 60 min.

2.3 Characterization

Glass granules (40 mg each) were subjected to DSC measurements (STA 449 F1, Netzsch, Germany) in the temperature range of 40-1000 ° C at a heating rate of 10 ° C/min in a flow of Ar. The obtained DSC curves were used to determine T_g, onset of crystallization (T_c), and peak of crystallization (T_p) (Table 3). The error in the determination of T_g, T_c, and T_p was estimated as ±2 ° C.

Amorphous and crystalline phases were analyzed by XRD (PANalytical X' Pert Pro, Netherlands) using a Cu K_α radiation source at 40 kV and 40 mA. Measurements were performed within the 2θ range of 10-80° at a scan rate of 2° /min and a step size of 0.013° /s. The crystallinities (X_c) of Schedule-I samples were calculated from the positions and relative intensities of their XRD peaks as follows:[23]

$$X_C = \frac{\Sigma I_{ci}}{\Sigma I_{ci} + K I_a} \times 100\%, \quad (1)$$

.

where I_a and I_{ci} are the integrated intensities of amorphous and crystalline phase peaks, respectively, while K is a constant that is related to the measurement conditions and glass composition (K = 0.963 for $Li_2Si_2O_5$ GCs).

Field-emission scanning electron microscopy (SEM; Hitachi S-4800, 5 kV, Japan) was used to observe phase separation before crystallization. The GC fracture surface was etched with 2 vol% aqueous HF for 25 s, cleaned by ultrasonication in deionized water for 10 min, and then sputter coated with platinum for 30 s to avoid the charging effect during SEM analysis.

Structural analysis was performed using a confocal laser Raman microscope (DXR, Thermo Electron, USA) equipped with a 532 nm laser operating at 100 mW. The spectra of quenched glasses with cleaned surfaces were acquired at 25 ° C in the wavenumber region of 100-1400 cm^{-1}. The signals at 850-1250 cm^{-1} were deconvoluted using Gaussian functions. Prior to deconvolution, spectra were normalized and the temperature and frequency dependency of the scattering intensity was corrected using a correction factor.[24]

3. Results

3.1 Thermal properties

The DSC curves of as-quenched and preheated glasses are shown in Figure 1. In the former case, the increase in T_g with increasing ZrO_2 content was attributed to the increase in network connectivity.[25] For P1Z0 exothermic peaks were

observed at 636 and 744 ° C which were shifted to higher temperatures for P1Z2. Specifically, the peak at 636 ° C shifted to 696 ° C and a small peak appeared near 655 ° C. The curve of P1Z4 showed only a small peak near 694 ° C, indicating that ZrO_2 inhibited glass crystallization for this composition. It is unclear if peak observed at ~655 ° C for P1Z2 represented glass crystallization, as it was less sharp than typical crystallization peaks. Similarly, the origin of the peak observed near 694 ° C for P1Z4 was also uncertain.

Since preheating promoted crystallization, the exothermic peaks of preheated samples were broader and located at lower temperatures compared to the as-quenched samples. For P1Z2, after 2 h of preheating at 560 ° C, the peak near 655 ° C significantly decreased and was not present after 4 h of preheating. In the case of P1Z4, preheating significantly reduced the intensity of the peak at approximately 694 ° C and resulted in the appearance of an exothermic peak near 850 ° C. Given that DSC is sensitive to the thermal history of samples and since fully crystallized samples do not exhibit crystallization peaks, the changes observed occurred during preheating.

3.2 Phase-separation behavior

The XRD patterns and Raman spectra of as-quenched and preheated glasses are shown in Figure 2. Excluding the P1Z0 sample preheated at 540 ° C for 4 h, all XRD patterns featured only amorphous phase peaks, indicating the absence of crystalline phases (Figure 2A). Essentially, P1Z2 and P1Z4 did not crystallize

.

during preheating and the small peak near 655 ° C in the DSC curve of P1Z2 is not attributable to crystallization. The peaks of P1Z0, preheated at 540 ° C for 4 h, were assigned to crystalline lithium metasilicate (Li_2SiO_3; PDF No. 29-0829) and this is further confirmed by the observation of peaks at 608 and 981 cm^{-1} in the corresponding Raman spectrum (Figure 2B).[26]

The major preheating-induced change in the Raman spectra is observed near 950 cm^{-1} (black dashed line in Figure 2B). With increasing preheating duration, the bands of P1Z0 and P1Z2 (initially at 958 cm^{-1}) shifted to 950 cm^{-1} and became sharper. In the case of P1Z4, after 4 h of preheating a sharp band at 950 cm^{-1} became more visible and was assigned to the characteristic [PO_4] group vibration[27]. Thus, preheating mainly resulted in structural changes in the phosphorus environment, which was predicted to be more ordered from the accumulation of orthophosphate units, as indicated by the peak sharpening of the 950 cm^{-1} peak.[10] Further discussion of the Raman spectra of the as-quenched glasses is presented in section 3.5.

3.3 Morphology

The SEM micrographs of as-quenched and preheated samples are shown in Figure 3. Prior to analyzing sample morphology, the ability of HF to easily erode phosphate-rich and lesser polymerized phases was confirmed. The HF-eroded areas were found to be rich in phosphorus and lithium since phosphorus is easily separated from the network and forms isolated orthophosphate groups which

.

attract Li^+ ions.[28, 29] All as-quenched glasses exhibited nanoscale granular or vermicular phase-separation structures with sizes of <20 nm. P1Z0 exhibited an interconnected morphology with closely clustered particles and poorly developed eroded ravines (Figure 3A). Compared to P1Z0, P1Z2 exhibited a partially interconnected morphology, with more pronounced eroded ravines and some isolated phase-separation droplets (Figure 3B); however, some traces of connectivity between droplets remained present. Conversely, P1Z4 featured a prominent phase-separation morphology with isolated droplets and clearly eroded ravines (Figure 3C). The addition of ZrO_2 affects the phase-separation morphology and results in an increased amount of separated phosphate-rich phases in as-quenched glasses.

With increased preheating time, the eroded ravines became more prominent in all cases, and isolated droplet phase-separation structures were observed after 4 h of preheating. As reported by Glatz *et al.*,[30] the separation of phosphate-rich phases is correlated to the nucleation of Li_2SiO_3 in LAS glasses with low Al_2O_3 content. Black erosion pits appeared between particles after 2 h of preheating (Figure 3D) and increased in size to ~30 nm after 4 h of preheating (Figure 3G). The erosion pits were associated with the Li_2SiO_3 crystals observed in Figure 2A, which were easily eroded by HF because of their low degree of polymerization.[22] More eroded areas were observed as the preheating time was increased (Figures 3H and 3I) and the corresponding XRD patterns and Raman spectra did not indicate nucleation and crystallization of Li_2SiO_3 (Figure 2). .

Furthermore, since HF mainly eroded phosphate-rich phases, it was concluded that preheating increased the content of these phases in P1Z2 and P1Z4. This behavior is consistent with the results of Raman spectroscopy (Figure 2B) which suggests that for P1Z2 and P1Z4, the preheating treatment induced changes in only the phosphorus environment. Therefore, the small peak near 655 ° C in the DSC curve of P1Z2 (Figure 2B) was attributed to increased phase separation.

3.4 Crystallization and primary phase evolution

Based on the significant difference between the DSC curves of P1Z0 and P1Z4, the effect of ZrO_2 on crystallization was mainly monitored for these compositions. During the heat treatment of P1Z0, both Li_2SiO_3 (PDF No. 29-0829) and $Li_2Si_2O_5$ (PDF No. 40-0376) crystals precipitated at 620 ° C and gradually grew until 680 ° C (Figure 4A). Upon further heating, $Li_2Si_2O_5$ crystal content rapidly increased, and at 750 ° C, Li_2SiO_3 crystals disappeared. Petalite ($LiAlSi_4O_{10}$; PDF No. 83-1470) crystals appeared at 700 ° C, became slightly more apparent with heating to 750 ° C, and then disappeared at 770 ° C. Another aluminum-containing crystal phase, β-quartz ss ($Li_xAl_xSi_{3-x}O_6$; PDF No. 31-0707), rapidly became more abundant above 720 ° C, developed into the main crystalline phase of the GC, and then transformed into β-spodumene ss ($Li_xAl_xSi_{3-x}O_6$; PDF No. 35-0794) at 820 ° C.[31]

The XRD pattern of P1Z4 heated at 680 ° C for 10 min exhibited peaks of Li_3PO_4 crystals at 33.9 and 36.5° (Figure 4B) that vanished as the crystallinity

.

increased. For P1Z4, Li_2SiO_3, $Li_2Si_2O_5$, $LiAlSi_4O_{10}$, and β-quartz ss, crystals precipitated at relatively higher temperatures. However, $LiAlSi_4O_{10}$ crystals did not disappear, and the transformation of β-quartz ss into β-spodumene ss was not observed in the investigated temperature range. Moreover, cristobalite (SiO_2; PDF No. 27-0605) crystals appeared at 720 ° C and increased until 750 ° C, then it decreased rapidly with the growth of $Li_2Si_2O_5$. As it has been reported that cristobalite precipitated during the transformation from Li_2SiO_3 into $Li_2Si_2O_5$.[9, 32]

The XRD patterns in Figure 5A reveal the first crystal phases to precipitate in P1Z0 and P1Z4 glasses. In P1Z0, precipitation preferentially resulted in Li_2SiO_3 and $Li_2Si_2O_5$ crystals, as reported by Huang *et al.*,[32] while Li_3PO_4 crystals preferentially precipitated in P1Z4. The Raman spectrum of P1Z0 heated at 575 ° C for 60 min (Figure 5B) exhibited bands of $Li_2Si_2O_5$ crystals[33] (at 414 and 1106 cm^{-1}) and peaks corresponding to the Si-O-Si vibration in crystalline Li_2SiO_3 (at 609 and 981 cm^{-1}).[26] The spectra of P1Z4 heated at 650 ° C for 30 and 60 min exhibited a sharp signal at 951 cm^{-1} attributed to Li_3PO_4 crystals with higher crystallinity.[34] This band was also observed for P1Z0, although no Li_3PO_4 peaks were observed in the corresponding XRD pattern, which may be owing to low crystallinity.

.

3.5 Glass structure

Figure 6 presents the Raman spectra of as-quenched glasses. The region between 400 and 600 cm^{-1} corresponds to the bending vibrations of the bridging oxygen (BO) bonds of SiO_4 tetrahedra.[35] The band near 490 cm^{-1} indicated the presence of four-membered rings, while the long tail at lower frequencies was attributed to the stretching vibration of oxygen bonds in high-membered rings.[36] The frequency changes in this region (marked with black arrows) are associated with silicate network deformation and ring statistic modification due to the presence of Zr atoms.[37] The band near 601 cm^{-1} was attributed to the rocking motion of bonds to BO in structural units containing non-bridging oxygen (NBO), which is characteristic of defect bonds in the silicate network.[38] With increasing ZrO_2 content, the intensity of this band (and hence the NBO content) decreased while the intensity of the band at 800 cm^{-1} remained nearly unchanged. For an enhanced illustration of the structural changes caused by ZrO_2, the high-frequency, unresolved group of bands over the 850-1250 cm^{-1} range was fitted using 4-6 Gaussian peaks (Figure 7) and the extracted parameters are listed in Table 4.

Peaks within the region of 850-1250 cm^{-1} conventionally correspond to the stretching vibrations of the Si-O bonds within SiO_4 tetrahedra. These are often described as Q^n units (where n is the number of BO atoms per tetrahedron), and provide important information on the glass structure.[39] For P1Z0, the peaks at 958, 1068, and 1152 cm^{-1} were assigned to the symmetric stretching vibrations of the Q^2, Q^3, and Q^4 units, respectively.[40] The peak at 1004 cm^{-1} was assigned .

as a T_2 vibrational mode of SiO_4 tetrahedra.[41] The peak at 957 cm^{-1} was attributed to the characteristic vibration of PO_4 tetrahedra, representing the structural environment of phosphorus in glass.[27] The peak near 990 cm^{-1} observed for P1Z2 and P1Z4 was assigned to the Si-O-Zr vibration in borosilicate glass by comparison with the Raman spectrum of zektzerite ($NaLiZrSi_6O_{15}$), in which Zr^{4+} ions are six-fold coordinated.[42] This band was assigned to one Si atom linked to three Si and one Zr (i.e., a ZrO_6 octahedra) neighboring atoms by BO atoms with Li^+ and Na^+ as charge-balancing cations. Therefore, the peak near 990 cm^{-1} was denoted as Q^3(Zr), while the peak at 1068 cm^{-1} was denoted as Q^3(Li). Zr can also connect with Q^2 units to form Q^2(Zr, Li) units. In contrast Si, Zr has a larger cationic radius (0.59 Å for Zr^{4+} *vs.* 0.26 Å for Si^{4+}) and atomic weight,[43] resulting in an elongation of the average T-O (T = Si, Zr) bond length. This accounts for the lower frequency of Q^3(Zr) units compared to Q^3(Li) units and the decrease in the frequency of Q^2 units.

Figure 8 shows the effects of ZrO_2 content on the relative areas of Raman bands, revealing that increasing ZrO_2 content resulted in a decrease in the combined area of Q^3(Li)+Q^4 and an increase in the area of Q^3(Zr). The increase in the number of Q^3(Zr) units reinforced the network as some Li^+ ions acted as charge-balancing cations of the ZrO_6 octahedra instead of engaging in network depolymerization through the formation of NBO in Q^3(Li) units. This effect of ZrO_2 on glass structure compensated for the decrease in the amount of Q^4 units, thereby increasing the degree of polymerization of the glass network.

With .

increasing ZrO_2 content, the area of PO_4 peaks slightly increased, while the peak position remained largely unchanged. The areal changes of the Q^2 and T_2 units are likely due to variation in the relative number of other units.

4. Discussion

4.1 Effect of ZrO_2 on crystallization behavior

DSC results indicate that glass crystallization was hindered by high ZrO_2 content, as reported previously.[19, 21] The DSC crystallization peak area is proportional to the remaining amount of residual glass, which depends on both the number of nuclei and the crystal growth rate.[44] In the DSC curve of as-quenched P1Z0, the area of the first crystallization peak decreased after addition of 1.8 mol% ZrO_2. While, Li_2SiO_3 and $Li_2Si_2O_5$ crystals precipitated preferentially in P1Z0, indicating the weakening of nucleation and crystal growth of Li_2SiO_3 and $Li_2Si_2O_5$ with the addition of ZrO_2. SEM and XRD data show that nucleation of Li_2SiO_3 only occurred in P1Z0 during preheating, and no crystal nuclei were observed in P1Z2 and P1Z4 even after 4 h of preheating in the common nucleation temperature range. As shown in Figure 4, the crystallization temperature of Li_2SiO_3 and $Li_2Si_2O_5$ increased by 100 ° C. The addition of ZrO_2 increases the polymerization degree of glasses, resulting in higher viscosity, thus, it hinders atomic diffusion and the increases. kinetic barrier of crystallization [21, 22] Additionally, the change of glass structure upon ZrO_2 incorporation also

.

contributed to this inhibitory effect. Indeed, the nucleation of Li_2SiO_3 is known to be sensitive to kinetic parameters.[45] Considering the nucleation process, Li_2SiO_3 is formed from both Q^2 and Q^3 units:[12]

$$Q^2 \text{ (glass)} \leftrightarrow Q^2 \text{ (crystal)}$$

$$2Q^3 \text{ (glass)} \leftrightarrow Q^2 \text{ (crystal)} + Q^4 \text{ (glass) [disproportionation]}$$

Based on the structural analysis, Zr can connect with Q^2(Li) units to form Q^2(Zr, Li) units and thus reduce the number of Q^2(Li) units available to directly forming Li_2SiO_3. Moreover, the Si-O-Zr bond is stronger than Si-O-Li bond, and the disproportionation reaction is suppressed because the P1Z4 network features more Q^3(Zr) units and fewer Q^3(Li) units. Consequently, the barrier towards nucleation of Li2SiO3 increases and a higher nucleation temperature is required. The crystallization of Li_2SiO_3 was reported to be closely related to that of $Li_2Si_2O_5$[9] which explains the suppression of glass nucleation and the increase in the crystallization temperatures of Li_2SiO_3 and $Li_2Si_2O_5$ with increasing ZrO_2 content.

The effects of heat treatment on the crystallinity of P1Z0 and P1Z4 are shown in Figure 9. The average grain size of Li_2SiO_3 crystals precipitated in P1Z0 and P1Z4 was calculated using the Scherrer equation. During the early stage of crystallization, the crystallinity of P1Z4 was lower than that of P1Z0, while the grain size of Li_2SiO_3 crystals in P1Z4 (~53 nm) exceeded that observed for P1Z0 (~21 nm). Thus, fewer Li_2SiO_3 crystals precipitated in P1Z4, which agrees .

with the proposed inhibitory effect of ZrO_2 on glass nucleation. Moreover, the highest crystallinity of P1Z4 was 18 % lower than that of P1Z0. Generally, when ZrO_2 is used as a nucleation agent in low-expansion LAS GCs, heterogeneous Zr-rich phase-separation droplets are preferentially formed during heat treatment which then gradually transform into ZrO_2 nanocrystals, providing heterogeneous nucleation sites.[18] Herein, no ZrO_2 precipitation was observed during the crystallization of P1Z4. Based on the lower crystallinity of P1Z4 and the presence of numerous residual glass phases therein, the ZrO_2 content did not reach saturation. Notably, P1Z4 contains a large amount of Li_2O which resulted in a lower degree of polymerization wherein ZrO_2 is more soluble.[46] Cormier *et al.*[47] suggested that the nucleation effect of Zr was caused by its distribution in the aluminosilicate matrix where direct connections between ZrO_x polyhedra are required for ZrO_2 to function as a nucleation agent. The linkages between these ZrO_x polyhedra increase the short-range order of the glass structure, leading to the separation of Zr-rich phases and the precipitation of ZrO_2 nuclei. However, the distribution of Zr is more regular in aluminosilicate glass networks with low degrees of polymerization.[48] Recently, Cicconi *et al.*[49] reported the occurrence of the sub-nano Zr local clusters in a Zr-rich SiO_2-Li_2O-P_2O_5-ZrO_2 glass having a SiO_2/Li_2O molar ratio < 2, while the local environment of Zr^{4+} is not dramatically changed during the different heat treatments, either when higher temperatures or longer times. This means that the connections between ZrO_x polyhedra are unlikely to form in P1Z4, or even

.

if Zr-rich clusters are formed, the absence of Zr-bearing crystals upon crystallisation of P1Z4 indicates that these aggregations do not evolve above the critical nucleus size. Consequently, ZrO_2 does not act as a nucleation agent in P1Z4.

4.2 Effect of ZrO_2 on phase-separation behavior

The separation of phosphate-rich phases or the formation of disordered Li_3PO_4 phases was reported to occur prior to the crystallization of Li_2SiO_3, and highly crystalline Li_3PO_4 was only formed at relatively higher temperatures.[12, 32] XRD and Raman spectroscopy revealed the preferential crystallization of Li_3PO_4 in P1Z4 (Figure 5). The relatively higher content of phosphate-rich regions in P1Z4 facilitated the crystallization of Li_3PO_4, as the composition prerequisites were fulfilled. Combining the results of SEM analysis and Raman fitting, the results indicate that ZrO_2 can promote phase separation by facilitating the separation of phosphate-rich phases. While it is known that ZrO_2 promotes the phase separation of Zr-rich droplets in low-expansion LAS GCs,[17, 18] there is no direct evidence that ZrO_2 promotes phase separation in Li_2O-Al_2O_3-SiO_2-P_2O_5-ZrO_2 glasses. The SEM results of as-quenched samples (Figure 3A-C) indicates that phase separation occurs spontaneously in the original glass composition. As the ZrO_2 content increased, phosphate-rich phases increased and gradually connected, which caused silicon-rich regions to appear as isolated droplets (Figure 3B-C). The kinetics of phosphate-rich phase separation is controlled by atomic

.

diffusion, thus, the temperature and time of heat treatment significantly affect the evolution of phase separation. With the extension of heat treatment time, the separated phosphate-rich phases increase, which is consistent with that observed in Figure 3D-I. Notably, the development of phase separation of samples containing ZrO_2 is more obvious, which indicates that ZrO_2 increases the immiscibility of glass.

The connection between Zr and the glass network has been found in several glass systems (e.g., borosilicate and aluminosilicate).[35, 42] In these glass networks, Zr^{4+} ions are nearly six-fold coordinated, and ZrO_6 octahedra share corners with SiO_4 or AlO_4 tetrahedra,[50, 51] as shown in Figure 10A. The origin of the promotional effect of ZrO_2 on the formation of phosphate-rich phases is illustrated by a structural scheme inspired by the models proposed by Quintas[42] and Greaves[52] (Figure 10B). As Zr enters the glass network, the solubility of phosphorus in the highly polymerized glass network decreases[28] and six-coordinated Zr is expected to preferentially bind to NBO.[48] The formation of Si-O-Zr linkages transforms a large number of Li^+ ions, that are combined with NBO as modifying ions, into charge-balancing ions. Thus, the mobility of Li^+ ions are increased. The yellow arrows in Figure 10B show that phosphorus attracts the charge-balancing ions of ZrO_6 polyhedra, inducing the aggregation of Li^+ ions in the network. As P^{5+} provides a stronger ionic field than Zr^{4+}, the former ion has a stronger ability to attract charge-balancing ions, while the coordination number of Zr may increase without sufficient charge-balancing .

ions. The isolated PO_4^{3-} units mainly occur in depolymerized regions. The dotted lines in Figure 10B indicate the separation between the depolymerized and polymerized regions, indicating the separation of phosphate-rich phases. Lin *et al.*[53] reported that in a binary lithium silicate glass, ZrO_2 promotes the separation of a depolymerized lithium-rich phase and a silicon-rich phase. Considering the affinity between phosphorus and lithium, the formation of separated phosphate-rich phases was expected in this study.

Phase separation is closely related to glass nucleation and the crystallization processes. Pre-crystallization phase separation during heat treatment has been observed for many glasses containing nucleation agents.[30, 54, 55] For example, when ZrO_2 and P_2O_5 are used as nucleation agents, they easily aggregate in the glass matrix to form a short-range-ordered structure which promotes phase separation. The phase boundary between the phase-separation region and matrix features a lower interfacial free energy, while the sharp concentration gradient at the interface facilitates atomic diffusion. In this study, ZrO_2 did not act as a nucleation agent but significantly promoted the development of phase separation during preheating. In the DSC results, the crystallization peaks of preheated samples shifted to relatively lower temperatures and the curve of P1Z4 exhibited an additional exothermic peak near 800 ° C, which indicated enhanced glass crystallization. Therefore, in the case of ZrO_2 and P_2O_5 co-doped LAS GC, ZrO_2 exhibited a dual effect. First, no phase separation of Zr-rich droplets or precipitation of ZrO_2 crystals occurred. Zr .

was connected to the network, mainly affecting nucleation kinetics, increasing glass viscosity, and inhibiting crystallization by forming strong network connections. Secondly, ZrO_2 promoted the separation of phosphorus-rich phase from the original glass phase and thus promoted crystallization. Although these two effects seem contradictory, both originate from the structural role of ZrO_2 in glass, with the inhibitory effect on nucleation kinetics having the dominant role at high ZrO_2 content. The dual effect of ZrO_2 found in this work provided new insights into the roles of ZrO_2 and P_2O_5 in low-Al_2O_3-content LAS GCs. The positive role of ZrO_2 on the crystallization was realized by the promoting effect on the separation of phosphorus-rich phase, rather than the nucleation of ZrO_2 itself. It indicated that appropriate ZrO_2/P_2O_5 ratio can minimize the inhibition of crystal growth and maximize the nucleation of P_2O_5, thus contribute to the formation of nanocrystals and fine microstructure of GCs.

5. Conclusion

The effect of ZrO_2 on the phase separation and crystallization in LAS glasses with low Al_2O_3 and P_2O_5 contents was studied. Thermal analysis showed that with increasing ZrO_2 content, the crystallization peaks shifted to relatively higher temperatures. For the glass containing 3.6 mol% ZrO_2 (P1Z4), the DSC curve was largely flat and a small crystallization peak was observed. The SEM and XRD results revealed that ZrO_2 hindered nucleation and reduced crystallinity. Higher ZrO_2 content favored the separation of phosphate-rich phases in as-quenched

.

glasses and the development of phase separation during preheating. The crystallization of Li_3PO_4 was observed at a relatively lower temperature in P1Z4, heated at 650 ° C for 30 min, owing to its abundant phosphate-rich phases. Raman spectrum fitting showed that Zr was mainly connected to the glass network through Si-O-Zr linkages, which significantly enhanced network connectivity. Structurally, we found that ZrO_2 had a dual effect. First, ZrO_2 inhibited crystallization by forming connections to the glass network that increased the viscosity and nucleation barrier of Li_2SiO_3, rather than resulting in the precipitation of ZrO_2 nanocrystals. Secondly, as Zr preferentially bonded to NBO, a sufficient amount of charge-balancing Li^+ ions existed in the network, which promoted the separation of phosphate-rich phases from the glass phase. Although this phase separation could improve glass crystallization, the dominant role of ZrO_2 was in the inhibition of glass crystallization. Thus, this study provides new insights into the roles of ZrO_2 and P_2O_5 in low-Al_2O_3-content LAS GCs.

.

Acknowledgement

This research study was funded by Xianning CSG Photovoltaic Glass Co., Ltd., [Grant No. XNGDJS2021082001]. The authors would also like to thank Dr. Jing Liu for SEM analyses performed at the State Key Laboratory of Advanced Technology for Materials Synthesis and Processing at Wuhan University of Technology, China.

References

1. Stookey SD. Catalyzed crystallization of glass in theory and practice. Ind. Eng. Chem. 1959;51(7):805-808.

2. Zanotto ED. A Bright Future for Glass-Ceramic. Am. Ceram. Soc. Bull. 2010;89(8):19-27.

3. Beall GH, Pinckney LR. Nanophase glass-ceramics. J. Am. Ceram. Soc. 1999;82(1):5-16.

4. Neuville DR, Cormier L, Ca Urant D, Montagne L, From glass to crystal. Nucleation, growth and phase separation: from research to applications. EDP sciences; 2017.

5. Huang SF, Li Y, Wei SH, Huang ZH, Gao W, Cao P. A novel high-strength lithium disilicate glass-ceramic featuring a highly intertwined microstructure. J. Eur. Ceram. Soc. 2017;37(3):1083-1094.

.

6. Arvind A, Tyagi AK, Mishra R, Shrikhande VK, Kothiyal GP. Evolution of crystalline phases as a function of composition and dwell time in lithium aluminium silicate glass-ceramics. Phys. Chem. Glasses-Eur. J. Glass Sci. Technol. B 2008;49(3):166-173.

7. Guo XZ, Yang H, Cao M. Nucleation and crystallization behavior of Li_2O-Al_2O_3-SiO_2 system glass-ceramic containing little fluorine and no-fluorine. J. Non-Cryst. Solids. 2005;351(24-26):2133-2137.

8. Höche T, Mäder M, Bhattacharyya S, Henderson GS, Gemming T, Wurth R, et al. $ZrTiO_4$ crystallisation in nanosized liquid-liquid phase-separation droplets in glass-a quantitative XANES study. Crystengcomm 2011;13(7):2550-2556.

9. Höland W, Apel E, van't Hoen C, Rheinberger V. Studies of crystal phase formations in high-strength lithium disilicate glass-ceramics. J. Non-Cryst. Solids. 2006;352(38-39):4041-4050.

10. Glatz P, Comte M, Cormier L, Montagne L, Doumert B, Moore GG. Different roles of phosphorus in the nucleation of lithium aluminosilicate glasses. J. Non-Cryst. Solids. 2018;493:48-56.

11. Rampf M, Fisch M, Helsch G, Deubener J, Ritzberger C, Höland W, et al. Quartz-containing glass-ceramics in the SiO_2-Li_2O-K_2O-MgO-CaO-Al_2O_3-P_2O_5 system. Int J Appl Glass Sci. 2019;10(3):330-338.

.

12. Bischoff C, Eckert H, Apel E, Rheinberger VM, Höland W. Phase evolution in lithium disilicate glass-ceramics based on non-stoichiometric compositions of a multi-component system: structural studies by ^{29}Si single and double resonance solid state NMR. Phys. Chem. Chem. Phys. 2011;13(10):4540-4551.

13. Huang SF, Zujovic Z, Huang ZH, Gao W, Cao P. Crystallization of a high-strength lithium disilicate glass-ceramic: An XRD and solid-state NMR investigation. J. Non-Cryst. Solids. 2017;457:65-72.

14. Lee SK, Stebbins JF. Al-O-Al and Si-O-Si sites in framework aluminosilicate glasses with Si/Al = 1: quantification of framework disorder. J. Non-Cryst. Solids. 2000;270:260-264.

15. Lee SK, Stebbins JF. Extent of intermixing among framework units in silicate glasses and melts. Geochim. Cosmochim. Acta 2002;66(2):303-309.

16. Kleebusch E, Patzig C, Hoche T, Russel C. A modified B_2O_3 containing Li_2O-Al_2O_3-SiO_2 glass with ZrO_2 as nucleating agent-Crystallization and microstructure studied by XRD and (S)TEM-EDX. Ceram. Int. 2018;44(16):19818-19824.

17. Kleebusch E, Patzig C, Höche T, Rüssel C. Phase formation during crystallization of a Li_2O-Al_2O_3-SiO_2 glass with ZrO_2 as nucleating agent-An X-ray diffraction and (S)TEM-study. Ceram. Int. 2017;43(13):9769-9777.

.

18. Kleebusch E, Patzig C, Krause M, Hu Y, Höche T, Rüssel C. The formation of nanocrystalline ZrO_2 nuclei in a Li_2O-Al_2O_3-SiO_2 glass-a combined XANES and TEM study. Sci. Rep. 2017;7(1).

19. Khalkhali Z, Ekta BE, Marghussian VK. Mechanical and Chemical Properties of Zr and P-Doped Lithium Disilicate Glass Ceramics in Dental Restorations. Int. J. Appl. Ceram. Tec. 2012;9(3):497-506.

20. Thieme K, Ruessel C. Nucleation and growth kinetics and phase analysis in zirconia-containing lithium disilicate glass. J Mater Sci. 2015;50(3):1488-1499.

21. Apel E, van't Hoen C, Rheinberger V, Höland W. Influence of ZrO_2 on the crystallization and properties of lithium disilicate glass-ceramics derived from a multi-component system. J. Eur. Ceram. Soc. 2007;27(2):1571-1577.

22. Krüger S, Deubener J, Ritzberger C, Höland W. Nucleation kinetics of lithium metasilicate in ZrO_2-bearing lithium disilicate glasses for dental application. Int J Appl Glass Sci. 2013;4(1):9-19.

23. Zheng X, Wen G, Song L, Huang XX. Effects of P_2O_5 and heat treatment on crystallization and microstructure in lithium disilicate glass ceramics. Acta Mater. 2008;56(3):549-558.

24. Long DA. Raman spectroscopy. New York: McGraw-Hill; 1977.

.

25. Matusita K, Sakka S, Maki T, Tashiro M. Study on crystallization of glass by differential thermal analysis. Effect of added oxide on crystallization of Li_2O-SiO_2 glasses. J Mater Sci. 1975;10:94-400.

26. Richet P, Mysen BO, Andrault D. Melting and premelting of silicates: Raman spectroscopy and X-ray diffraction of Li_2SiO_3 and Na_2SiO_3. Phys. Chem. Miner. 1996;23(3):157-172.

27. Popović L, Manoun B, de Waal D, Nieuwoudt MK, Comins JD. Raman spectroscopic study of phase transitions in Li_3PO_4. J. Raman Spectrosc. 2003;34(1):77-83.

28. Mysen BO, Ryerson FJ, Virgo D. The structural role of phosphorus in silicate melts. Am. Mineral. 1981;66:106-117.

29. O'Donnell MD, Watts SJ, Law RV, Hill RG. Effect of P_2O_5 content in two series of soda lime phosphosilicate glasses on structure and properties-Part I: NMR. J. Non-Cryst. Solids. 2008;354(30):3554-3560.

30. Glatz P, Comte M, Montagne L, Dountert B, Cousin F, Cormier L. Structural evolution at short and medium range distances during crystallization of a P_2O_5-Li_2O-Al_2O_3-SiO_2 glass. J. Am. Ceram. Soc. 2020;103(9):4969-4982.

31. McMillan PW. Glass Ceramics. New York: Academic Press; 1979.

32. Huang SF, Cao P, Li Y, Huang ZH, Gao W. Nucleation and crystallization kinetics of a multicomponent lithium disilicate glass by in situ and real-time synchrotron X-ray diffraction. Cryst. Growth Des. 2013;13(9):4031-4038. .

33. Fuss T, Moguš-Milanković A, Ray CS, Lesher CE, Youngman R, Day DE. Ex situ XRD, TEM, IR, Raman and NMR spectroscopy of crystallization of lithium disilicate glass at high pressure. J. Non-Cryst. Solids. 2006;352:4101-4111.

34. Kowada Y, Tatsumisago M, Minami T. Raman spectra of rapidly quenched glasses in the systems lithium borate-lithium silicate-lithium phosphate (Li_3BO_3-Li_4SiO_4-Li_3PO_4 and $Li_4B_2O_5$-$Li_6Si_2O_7$-$Li_4P_2O_7$). J. Phys. Chem. 1989;93(5):2147-2151.

35. Ficheux M, Burov E, Aquilanti G, Trcera N, Montouillout V, Cormier L. Structural evolution of high zirconia aluminosilicate glasses. J. Non-Cryst. Solids. 2020;539:120050.

36. Galeener FL. Planar Rings in Vitreous Silica. J. Non-Cryst. Solids. 1982;49(1-3):53-62.

37. Lu X, Deng L, Gin S, Du J. Quantitative Structure-Property Relationship (QSPR) Analysis of ZrO_2-Containing Soda-Lime Borosilicate Glasses. J. Phys. Chem. B 2019;123(6):1412-1422.

38. Brawer SA, White WB. Raman spectroscopic investigation of the structure of silicate glasses (II). Soda-alkaline earth-alumina ternary and quaternary glasses. J. Non-Cryst. Solids. 1977;23(2):261-278.

39. McMillan P. Structural studies of silicate glasses and melts-applications and limitations of Raman spectroscopy. Am. Mineral. 1984;69(6):622-644.

.

40. Mysen BO, Virgo D, Kushiro I. The structural role of aluminum in silicate melts-a Raman spectroscopic study at 1 atmosphere. Am. Mineral. 1981;66:678-701.

41. Le Losq C, Neuville DR, Florian P, Henderson GS, Massiot D. The role of Al^{3+} on rheology and structural changes in sodium silicate and aluminosilicate glasses and melts. Geochim. Cosmochim. Acta. 2014;126:495-517.

42. Quintas A, Caurant D, Majérus O, Loiseau P, Charpentier T, Dussossoy JL. ZrO_2 addition in soda-lime aluminoborosilicate glasses containing rare earths: Impact on the network structure. J. Alloys Compd. 2017;714:47-62.

43. Shannon RD. Revised effective ionic radii and systematic studies of interatomic distances in halides and chalcogenides. Acta Cryst 1976;32:751-767.

44. Zheng Q, Zhang Y, Montazerian M, Gulbiten O, Mauro JC, Zanotto ED, et al. Understanding Glass through Differential Scanning Calorimetry. Chem. Rev. 2019;119(13):7848-7939.

45. Gaddam A, Fernandes HR, Tulyaganov DU, Ribeiro MJ, Ferreira JMF. The roles of P_2O_5 and SiO_2/Li_2O ratio on the network structure and crystallization kinetics of non-stoichiometric lithium disilicate based glasses. J. Non-Cryst. Solids. 2018;481:512-521.

46. Kato K, Araki N. The corrosion of zircon and zirconia refractories by molten glasses. J. Non-Cryst. Solids. 1986;80:681-687.

.

47. Cormier L, Dargaud O, Calas G, Jousseaume C, Papin S, Trcera N, et al. Zr environment and nucleation role in aluminosilicate glasses. Mater. Chem. Phys. 2015;152:41-47.

48. Frages F, Ponader CW, JR. GEB. Structural environments of incompatible elements in silicate glass/melt systems-Zirconium at trace levels. Geochim. Cosmochim. Acta. 1991;55:1563-1574.

49. Cicconi MR, Belli R, Brehl M, Lubauer J, Hayakawa T, Kimura K, et al. Nucleation mechanisms in a SiO_2-Li_2O-P_2O_5-ZrO_2 biomedical glass-ceramic: Insights on crystallisation, residual glasses and Zr^{4+} structural environment. J. Eur. Ceram. Soc. 2022;42(4):1762-1775.

50. Ferlat.G, Cormier.L, Thibault MH, Galoisy.L, Calas.G, Delaye JM, et al. Evidence for symmetric cationic sites in zirconium-bearing oxide glasses. Phys. Rev. B 2006;73:214207.

51. Jollivet P, Calas G, Galoisy L, Angeli F, Bergeron B, Gin S, et al. An enhanced resolution of the structural environment of zirconium in borosilicate glasses. J. Non-Cryst. Solids. 2013;381:40-47.

52. Greaves GN. EXAFS and the structure of glass. J. Non-Cryst. Solids. 1985;71:203-217.

53. Lin CC, Shen P, Chang HM, Yang YJ. Composition dependent structure and elasticity of lithium silicate glasses: Effect of ZrO_2 additive and the

.

combination of alkali silicate glasses. J. Eur. Ceram. Soc. 2006;26(16):3613-3620.

54. Barry TI, Clinton D, Lay LA, Mercer RA, Miller RP. The crystallizaion of glasses based on eutectic compositions in the system Li_2O-Al_2O_3-SiO_2. J Mater Sci. 1969;4:596-612.

55. Kleebusch E, Patzig C, Hoche T, Russel C. The evidence of phase separation droplets in the crystallization process of a Li_2O-Al_2O_3-SiO_2 glass with TiO_2 as nucleating agent An X-ray diffraction and (S)TEM-study supported by EDX-analysis. Ceram. Int. 2018;44(3):2919-2926.

.

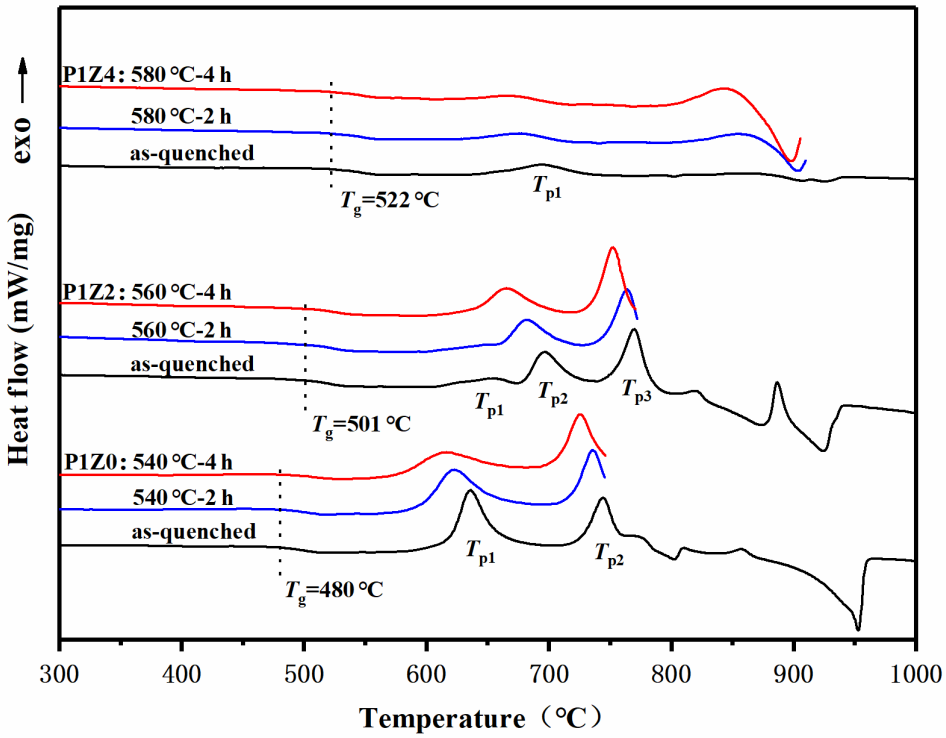

Figure 1. DSC curves of as-quenched and preheated samples according to Schedule I.

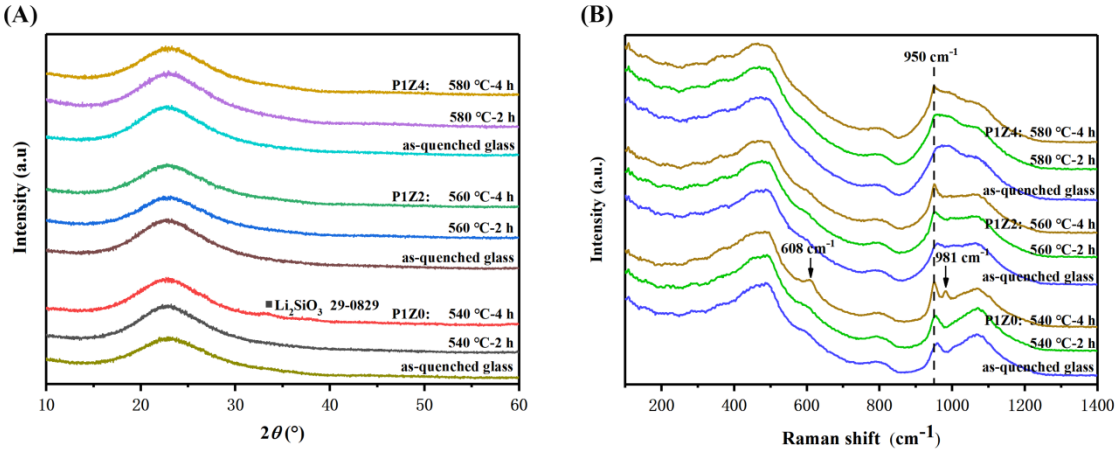

Figure 2. (A) XRD patterns and (B) Raman spectra of as-quenched and preheated samples.

.

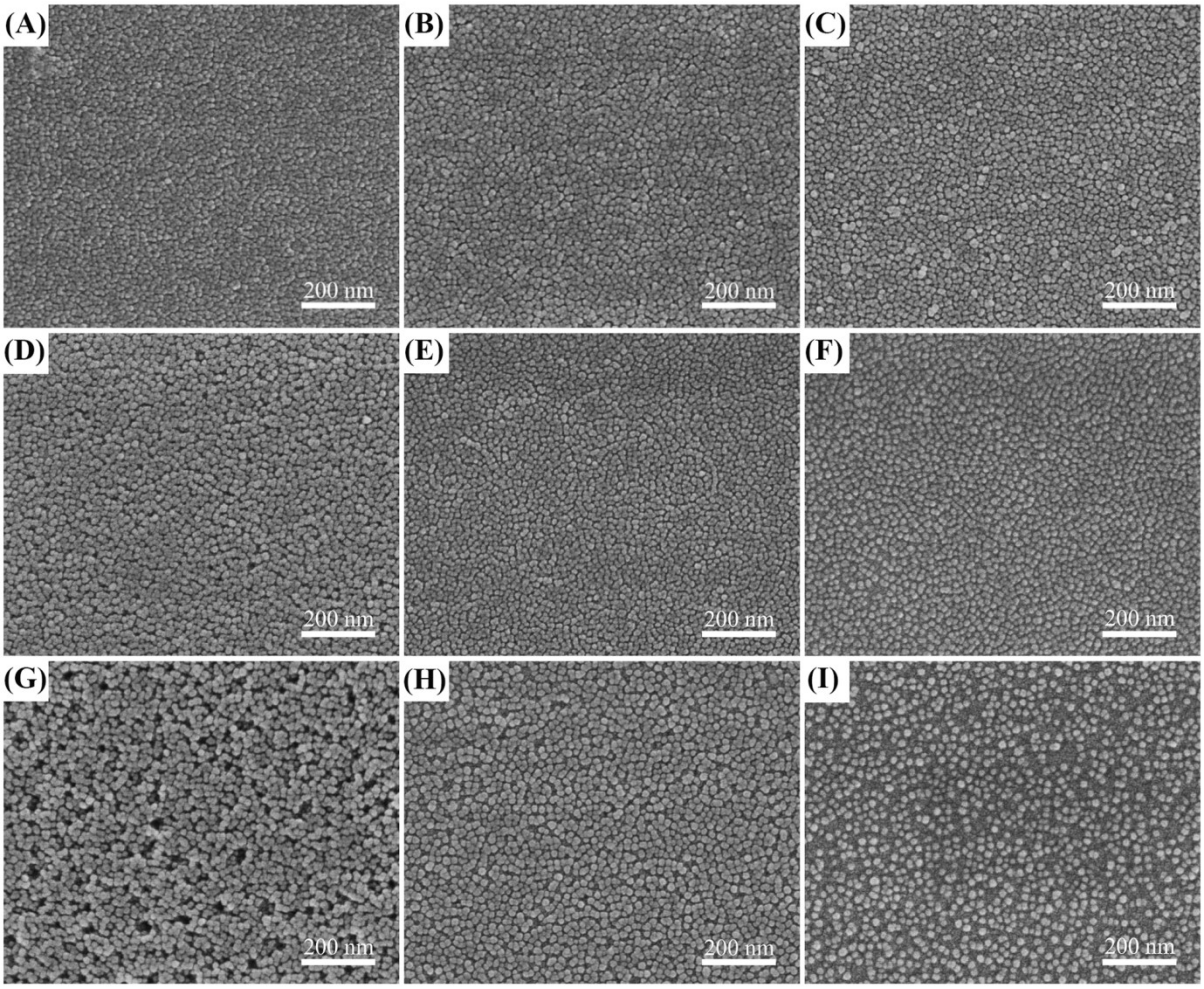

Figure 3. Micrographs of (A-C) as-quenched [A: P1Z0; B: P1Z2, C: P1Z4] and (D-I) preheated [D: P1Z0 (540 ° C for 2 h); E: P1Z2 (560 ° C for 2 h); F: P1Z4 (580 ° C for 2 h); G: P1Z0 (540 ° C for 4 h); H: P1Z2 (560 ° C for 4 h); I: P1Z4 (580 ° C for 4 h)] samples etched with 2 wt% HF.

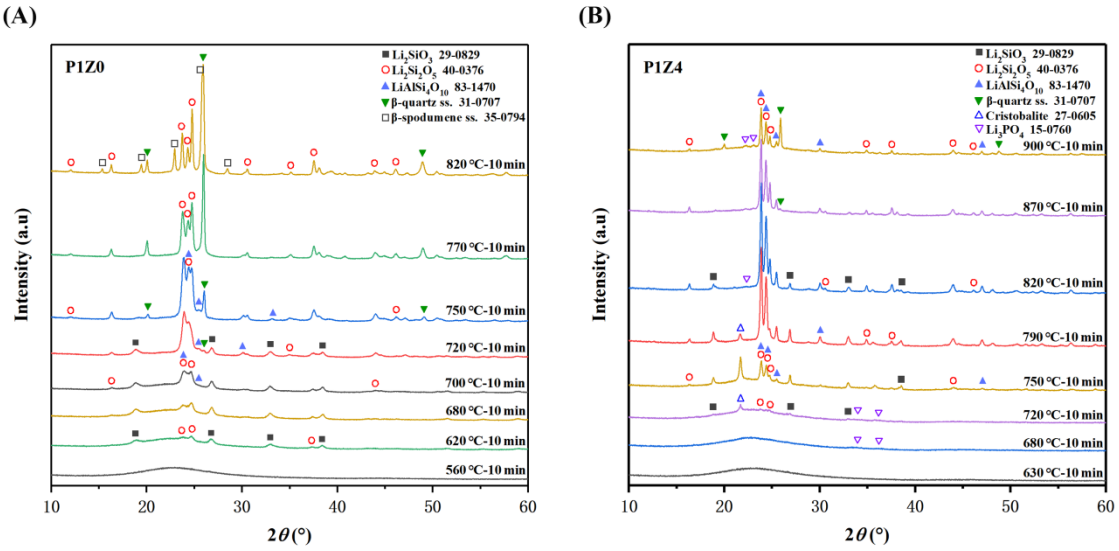

Figure 4. XRD patterns of (A) P1Z0 heat-treated from 560 to 820 ° C for 10 min and (B) P1Z4 heated-treated from 630 to 900 ° C for 10 min according to Schedule Ⅱ.

.

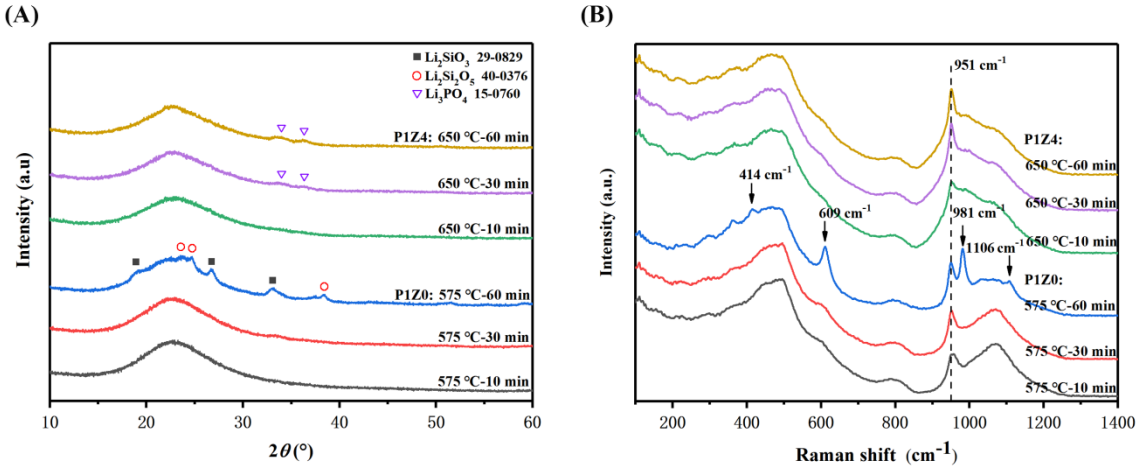

Figure 5. (A) XRD patterns and (B) Raman spectra of P1Z0 and P1Z4 heat-treated according to Schedule Ⅲ.

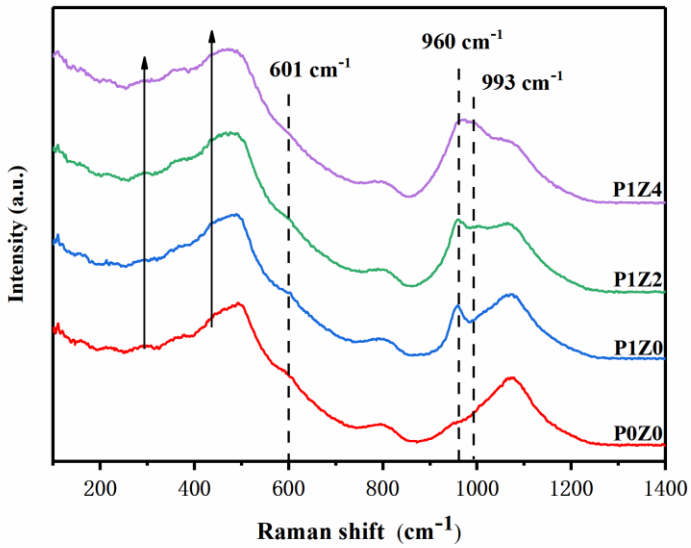

Figure 6. Raman spectra of as-quenched samples.

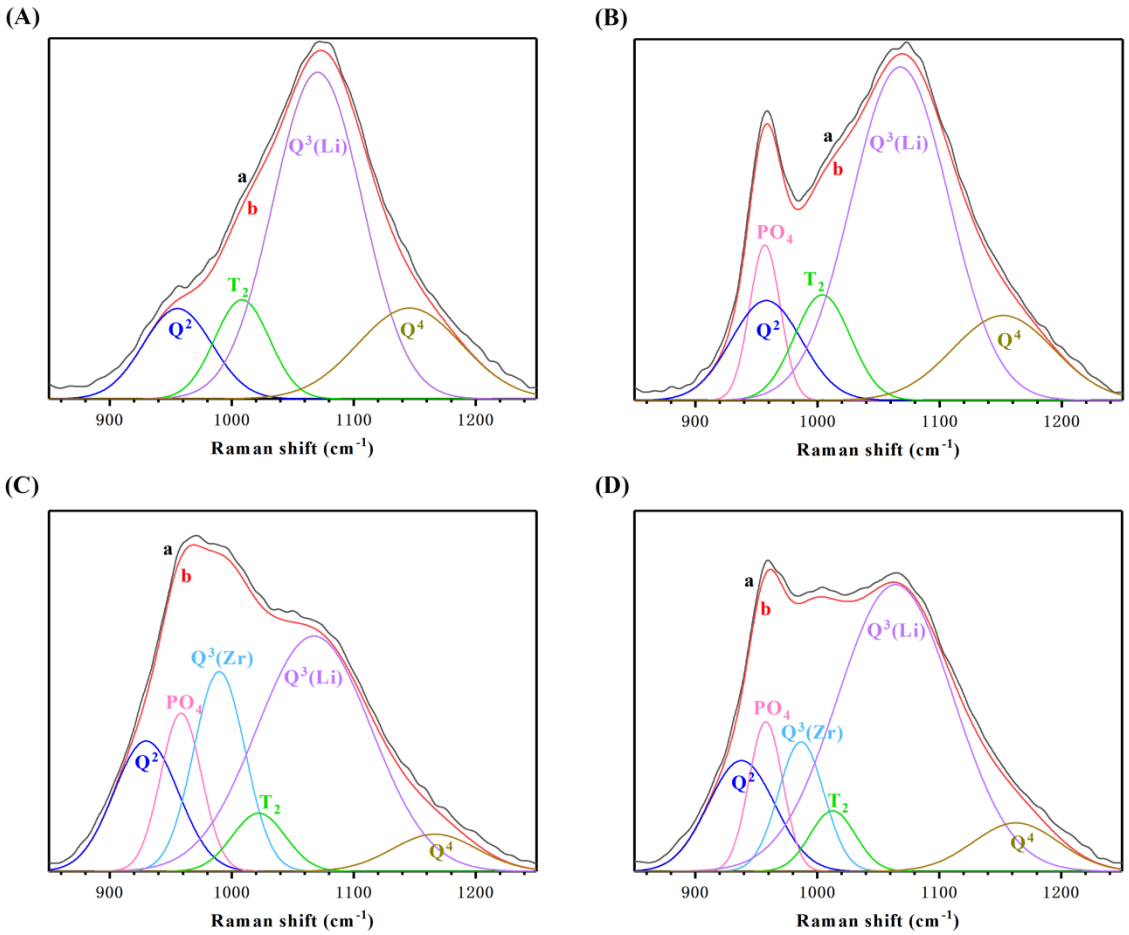

Figure 7. Deconvoluted Raman spectra of (A) P0Z0, (B) P1Z0, (C) P1Z2, and (D) P1Z4. Experimental spectra (a) are slightly shifted towards the top of the Gaussian fitting (b).

.

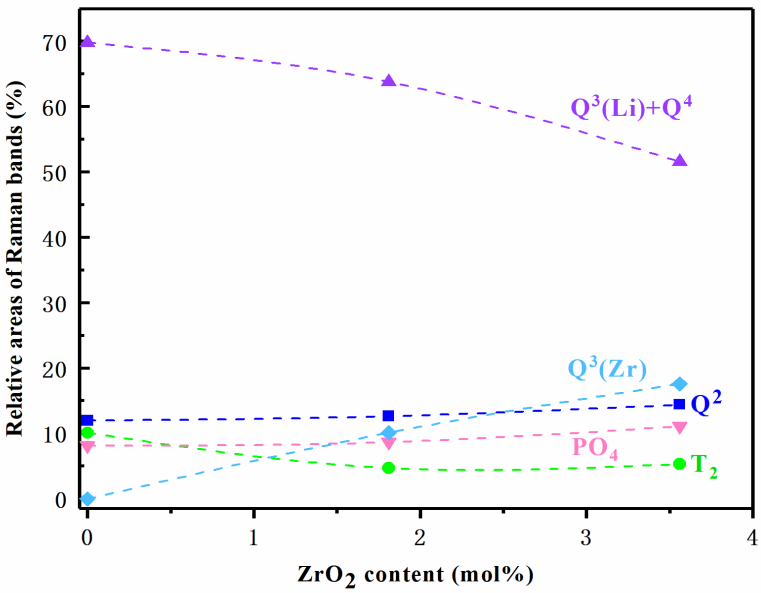

Figure 8. Effects of ZrO_2 content on the normalized relative areas of fitted Raman bands.

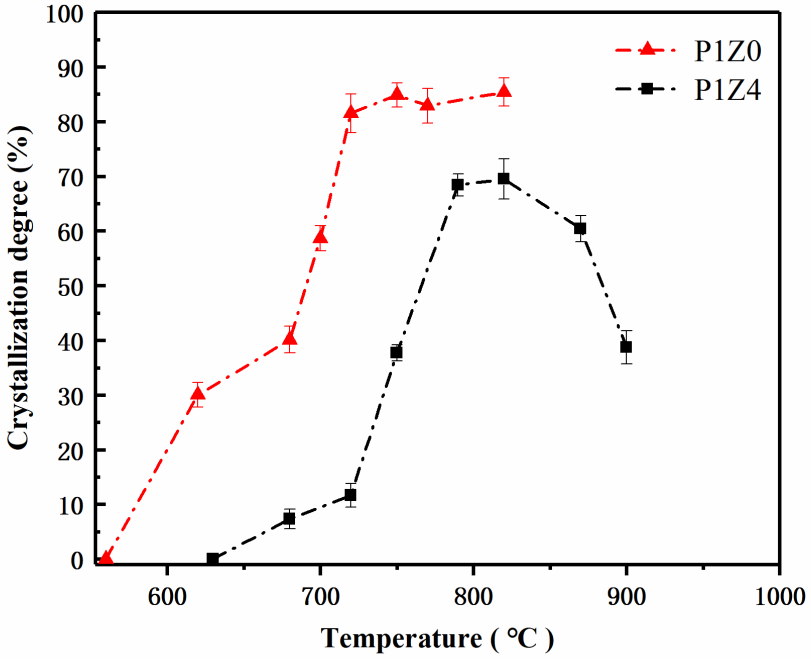

Figure 9. Crystallinities (%) of P1Z0 and P1Z4 heat-treated according to Schedule Ⅱ.

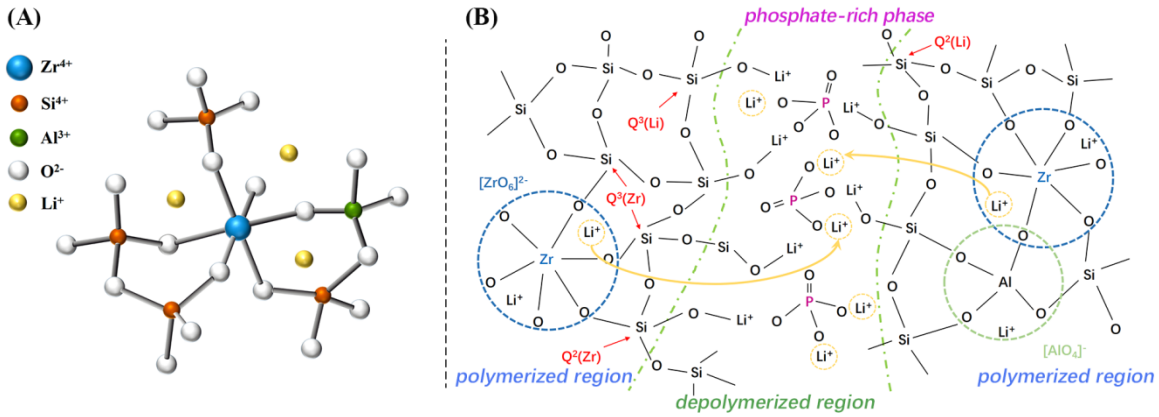

Figure 10. (A) Stereoscopic structural diagram of the connections between ZrO_6 octahedra and SiO_4 or AlO_4 tetrahedra with local charge compensation by Li^+ ions. (B) Schematic bidimensional representation of the structure of a ZrO_2-containing glass.

Tables

Table 1. Nominal (in parentheses) and actual glass compositions, mol%.

Glass	SiO_2	Al_2O_3	P_2O_5	Li_2O	ZrO_2
P1Z0	72.5(72.65)	5.1(5.00)	0.91(0.85)	20.1(21.50)	0(0)
P1Z2	71.1(71.33)	4.9(4.91)	0.85(0.83)	19.9(21.13)	1.7(1.8)
P1Z4	70.3(70.02)	4.9(4.82)	0.80(0.82)	19.5(20.74)	3.6(3.6)
P0Z0	73.2(73.50)	4.8(5.00)	0.09(0)	20.5(21.50)	0(0)

Table 2. Heat treatment conditions.

	Schedule	Temperature (℃)	Time (min)
P1Z0	I	540	240, 480
	II	560, 620, 680, 700, 720, 750, 770, 820	10
	III	575	10, 30, 60
P1Z2	I	560	240, 480
	I	580	240, 480
P1Z4	II	630, 680, 720, 750, 790, 820, 870, 900	10
	III	650	10, 30, 60

Table 3. Characteristic temperatures (±2 ° C) determined by DSC, ° C.

Glass	T_g	T_{c1}	T_{p1}	T_{c2}	T_{p2}	T_{c3}	T_{p3}
P1Z0*	480	594	636	714	744	-	-
P1Z2*	501	-	655	674	696	740	769
P1Z4	522	-	694	-	-	-	-

* 1, 2 and 3 in the subscripts of T_{cx} and T_{px} refer to the order of peaks.

Table 4. Raman shifts (cm^{-1}), relative areas (%), and full-widths at half maximum (FWHM, cm^{-1}) of peaks obtained after the deconvolution of Raman spectra.

	Q^2	T^2	Q^3	Q^4	PO_4	$Q^3(Zr)$
Raman shift						
P0Z0	956	1009	1071	1146	-	-
P1Z0	958	1004	1068	1152	957	-
P1Z2	938	1013	1064	1163	958	988
P1Z4	930	1022	1067	1167	957	989
Relative area						
P0Z0	12.41	10.88	58.11	18.67	-	-
P1Z0	11.98	10.11	55.29	14.51	8.13	-
P1Z2	12.64	4.73	56.75	7.08	8.67	10.12
P1Z4	14.42	5.34	46.21	5.38	11.12	17.61
FWHM						
P0Z0	66.5	53.1	86.1	100.3	-	-
P1Z0	67.9	54.1	93.8	97.6	29.6	-
P1Z2	64.4	44.1	111.7	82.9	32.8	44.1
P1Z4	62.5	51.7	110.9	82.2	39.7	49.8